J. Hydrol. Hydromech., 61, 2013, 3, 222–231
DOI: 10.2478/johh-2013-0029

Shape of the nappe during free overfall from a rectangular channel with zero bed slope

Zbyněk Zachoval *, Petr Böhm, Jana Pařílková, Robert Šafář, Jan Šulc

Brno University of Technology, Faculty of Civil Engineering, Veveří 331/95, 602 00 Brno, Czech Republic.
* Corresponding author. E-mail: zachoval.z@fce.vutbr.cz

Abstract: The paper deals with selected procedures used to calculate the shape of compact nappe during free overfall from a smooth horizontal channel with rectangular cross section. Calculated and measured water surface and velocity conditions in the end section, the level of water surface upstream in front of the end section and the shape of the compact part of an overfall nappe are described for a particular compared case.

Keywords: Nappe shape; End depth; Free overfall; Confined nappe; Unconfined nappe; Numerical modelling; Experimental measurement.

INTRODUCTION

The determination of the shape of a nappe during free overfall from a channel, e.g. with rectangular cross section, is an important part of construction design in many practical applications. These are sudden drops in the channel bed, flumes and channels with a sudden end of the bed, culverts with outflow into a free space, certain sewerage and roof inlets, measuring flumes for determining the discharge Q using the measured end depth h_e, broad-crested weirs, etc.

During the flow of water in a channel near the end section when the curvature of streamlines can be neglected, the hydraulic calculation of the shape of the compact part of a nappe (without air entrainment) is relatively well explained (Kolář et al., 1983; Wahl et al., 2008), but less explained with self aeration (Falvey, 1980). This concerns cases with a supercritical regime when the assumption of the non-curvature of streamlines is fulfilled and, at the same time, the flow is without air entraimnment. These are, e.g., short chutes, spillway conduits and straight drop structures.

Flow in a channel near the end section where curvature of streamlines cannot be neglected concerns channels with an approximately zero bed slope. There are many approaches for solving that flow like a one-dimesional (1D), two-dimensional (2D) and three-dimensional (3D), but with different accuracy. This paper is focused on comparing its results with the measurements.

FREE OVERFALL FROM A CHANNEL

Overfall from a channel forms a relatively extensive part of hydraulics. Research has gradually divided the issue according to the location of the end section into front and side overfalls; according to the effect of tailwater into free and submerged overfalls; and according to the longitudinal shape of the channel into overfall form prismatic and non-prismatic channels (Beirami et al., 2006).

In the case of the front overfall, prismatic channels are divided by the shape of their cross section (ISO 3847, 1977), (ISO 4371, 1984) into channels with rectangular (square or oblong) profiles and those with non-rectangular (trapezoidal, triangular (Dey and Kumar, 2002), circular (Dey, 2002a), semicircular (Dey, 2001; Raikar et al., 2004), parabolic and other (Dey and Lambert, 2007)) profiles. Moreover, channels can be divided using the bed slope i_0 into channels with a negative slope, a zero slope and a positive slope (Dey, 2000). A special case is division by the properties of the channel surface (Bos, 1989) expressed, e.g., by the roughness coefficient (Firat, 2004), or by the friction coefficient (Dey, 2000) determined on the basis of the relative roughness of the channel (Pařílková et al., 2012). The overfall nappe can be divided into confined (side-bounded) and unconfined (side-unbounded) nappes (ISO 3847, 1977).

Due to the extent of the issue, it is considered having only a front free overfall from a smooth horizontal prismatic channel of a rectangular cross section of the width b, when water movement is caused only by forces of gravity determined by the gravitational acceleration g (constant). The hydraulic calculation of flow in the channel with end section is relatively complicated. Due to the curvature of streamlines, the critical depth h_c (it is assumed that the distribution of velocities over the cross section is constant, $\alpha = 1.0$)

$$h_c = \left(\frac{\alpha Q^2}{g b^2} \right)^{1/3} \tag{1}$$

does not form at the end section, but at a certain distance L_c upstreame. At the end section, the so-called end depth h_e is created, being smaller than the critical depth: $h_e < h_c$. The ratio between the end depth and the critical depth is called the "end-depth ratio" (EDR) (Dey, 2002)

$$EDR = \frac{h_e}{h_c} . \tag{2}$$

The curvature of streamlines in the area between the section with the critical and end depths is relative to depth. The curvature is zero at the channel bed and maximal on the water surface; in this case, the hydrostatic distribution of the pressure p across the flow depth h is not applied. The dimensionless depiction of the overfall in its longitudinal plane of symmetry determined by the axes Z/h_c and X/h_c is shown in Fig. 1.

The 1D calculation of the entire phenomenon is usually divided into three parts. The first part includes the calculation of flow in the area of the channel before the critical depth h_c, the second part forms the calculation of flow between the critical

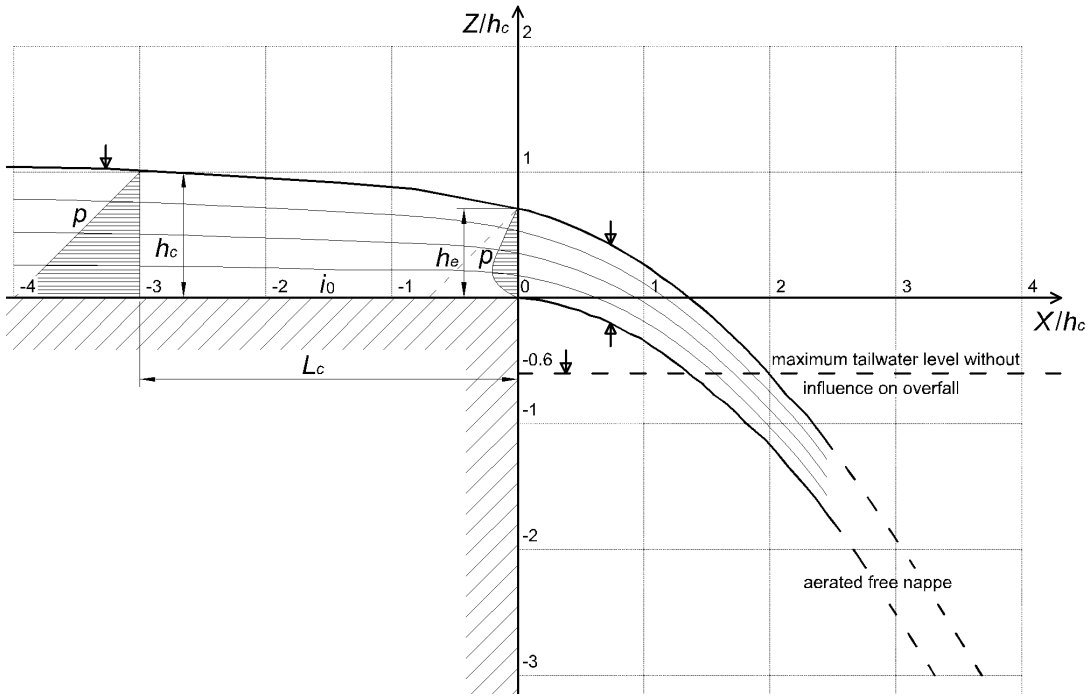

Fig. 1. Longitudinal vertical section through the plane of symmetry of the free overfall with an unconfined nappe and with the designation of variables.

depth h_c and the end depth h_e, and the third part is the calculation of the shape of a free overfall nappe.

The 1D calculation of flow before the critical depth h_c is well explained. To solve it, a step method – the standard step method – is most often used (Chow, 1959; Kolář et al., 1983); when calculating it, it is proceeded upstream from the profile with the critical depth h_c determined by the Eq. (1).

The place of the origin of the critical depth h_c, determined by the length L_c, or by their ratio L_c/h_c, is generally variable, depending particularly on the bed slope i_0 (Dey, 2002), or on the value of the Froude number Fr (Dey, 2002), the shapes of the longitudinal and cross sections of the channel and on the relative roughness k_s/R, where k_s is the equivalent Nikuradse sand-grain roughness height and R is the hydraulic radius. In the case of the prismatic rectangular channel with a zero bed slope, the critical depth is at a distance $L_c = 3h_c$ to $4h_c$ from the end section (Chow, 1959).

The description of flow between the critical depth h_c and the end depth h_e and the indication of their ratio *EDR* (2) is the subject of about 80 years long investigation that has probably not finished yet which show numerous new papers (Castro-Orgaz and Hager, 2010; Sharifi et al., 2010; Castro-Orgaz and Hager, 2011). The methods of the solution of flow in this interval can be divided (Dey, 2002) into: the Boussinesq approximation (Dey, 2002), the energy approach (Anderson, 1967; Haeger, 1983), the momentum approach (Murty Bhallamudi, 1994), the weir (without crest) flow approach (Rouse, 1936), the free-vortex approach (Ali and Sykes, 1972), the potential flow approach (Southwell and Vaisey, 1946) and empirical approach (Davis et al., 1998).

The value of the end depth h_e is not generally dependent only on the discharge Q, the gravitational acceleration g and the width b of the channel, but also on the shape of the longitudinal and cross sections of the channel (Ferro, 1999), the slope i_0 of the channel bed, the relative roughness k_s/R of the channel (Firat, 2004), on the side boundaries of the nappe and, for the end depths $h_e < 0.03$ m (Bos, 1989), also on the Weber number We and the Reynolds number Re.

The end depth h_e can also be used for determining the discharge Q. In a channel of a rectangular cross section of the width b with the zero bed slope i_0 and with the action of gravitational acceleration g, on the basis of the knowledge of the value of the end depth h_e, the equation below is used (ISO 3847, 1977)

$$Q = C_d \mathrm{g}^{1/2} b h_e^{3/2}, \tag{3}$$

where C_d is the discharge coefficient ($C_d = 1.66$ for a confined nappe, $C_d = 1.69$ for an unconfined nappe; $b > 0.3$ m, $h_e > 0.04$ m (ISO 3847, 1977)). For non-rectangular cross sections of a channel, the Eq. (3) is somewhat more complicated (practically every shape of the cross section has its own equation), being based on the critical depth h_c with the indication of *EDR* (ISO 4371, 1984).

The methods of flow description mentioned above can be used particularly for determining the ratio *EDR*. In the area of description of the trajectory and shape of a free overfall nappe, they cannot be used generally. The trajectory of a free overfall nappe was discussed in White et al. (1943), Markland (1965), Marchi (1993), Davis et al. (1999), Wahl et al. (2008), Hong et al. (2010) and others. Particularly a confined and fully aerated nappe is described to a distance before it is compact. Valuable information can be obtained from the Straight Drop Structure Design Guidelines from 1991 (Standing Committee on Rivers and Catchments, 1991) in which the mean shape of the upper and lower surface of a free nappe and his trajectory under the tailwater surface level Z_d is depicted. The relationship is redrawn in Fig. 2 which indicates points of the tangential deviation of the upper surface of the nappe in the place of the tailwa-

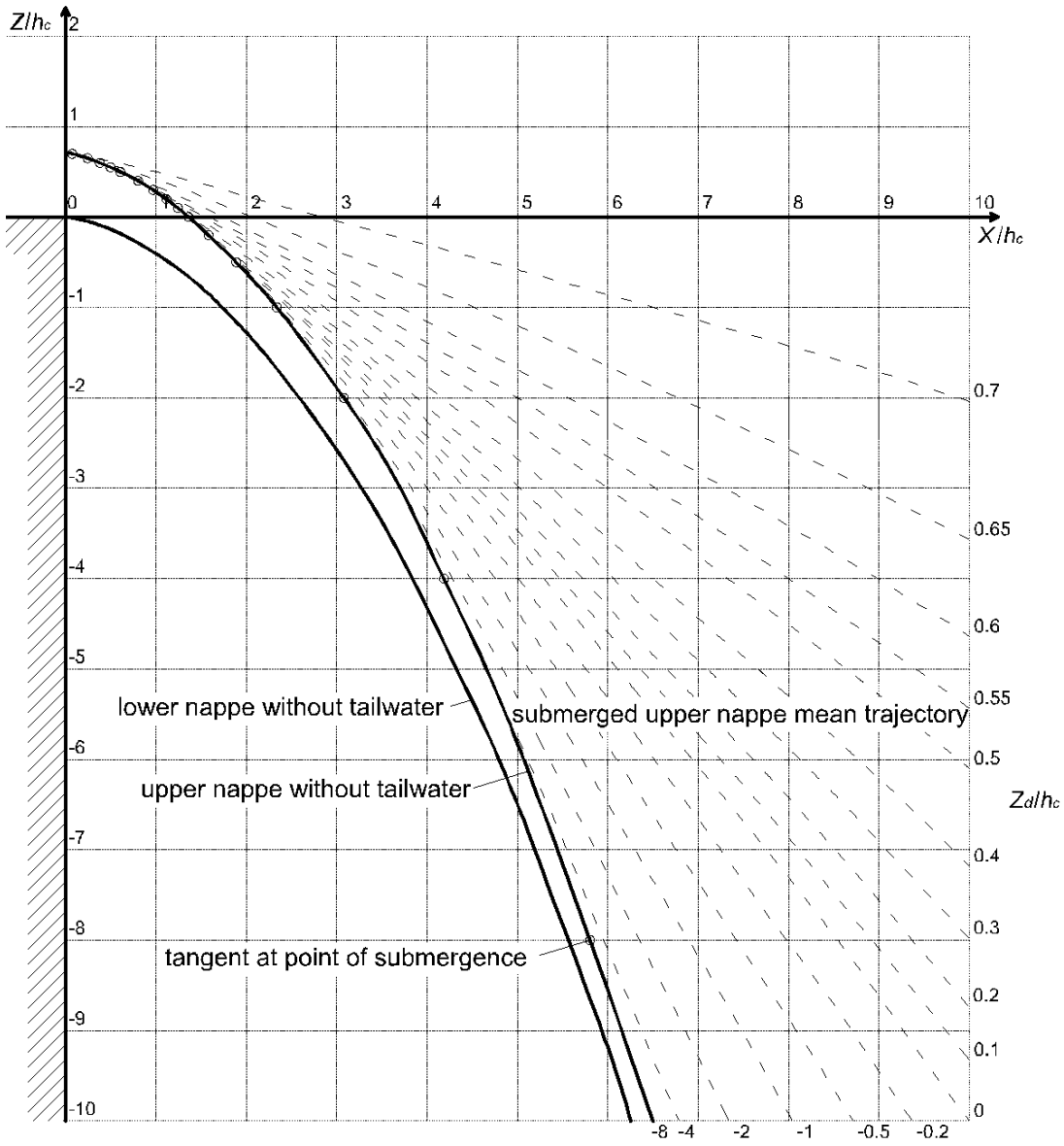

Fig. 2. Shape of a confined overfall nappe after the Straight Drop Structure Design Guidelines (Standing Committee on Rivers and Catchments, 1991), redrawn from the original.

ter level; the trajectories marked by a dashed line are used, e.g., to design the shape of a stilling pool (the nappe breaks down under the tailwater surface level).

This overview shows that in the case of a complete description of the phenomenon it is necessary to make practically always three separate consecutive calculations, which can be relatively complicated. Disadvantages of this calculation separation are eliminated by a 2D or a 3D solution by means of a numerical model (Wang et al., 2009) using the Reynolds equations, which provides a complete view of flow (velocities and pressures) (Ramamurthy et al., 2006). At the present time, free overfall from a channel of a rectangular cross section with a confined and fully aerated nappe is used as a testing or a validating task of numerical models, e.g. Zerihun and Fenton (2004), Jia and Wang (2005), Wang et al. (2009), etc. This paper deals particularly with this solution for a confined as well as an unconfined nappe. There are not many measured data suitable for comparing the shape of an unconfined nappe; hence a physical experiment was used.

PHYSICAL EXPERIMENT

The channel with length 2.5 m and square cross section of 0.15 m in width and height was used. In the inlet were regulating wings and polystyrene slab for faster stabilisation of flow. The channel was ended in the cross section perpendicular to its longitudal axis (Fig. 3).

The determination of discharge was made using a Thomson weir. Water falling from the channel freely without side walls; hence this was an unconfined nappe. This physical experiment is described in more detail in Böhm (2010).

The position of the water surface was measured by a point contact gauge with three exchangeable needle points. Velocities were measured by a UVP Monitor XW-PSi instrument with a 4-MHz probe.

The system of coordinates chosen for determining the shape of the water surface its origin in the centre of the end edge, the axis X was oriented horizontally downstream, the axis Y passed through the end edge and the axis Z was vertical (positive upwards).

Fig. 3. Physical experiment (left), a point contact gauge (right).

Assumptions were the symmetrical distribution of the velocity field about the plane *XZ*, which was confirmed by testing measurement, and negligible velocities in the direction of the axis *Y*. Instantaneous point velocities u_x in the direction of flow and at the end section (Fig. 5) were measured upwards from a distance of 0.04 m in front of the end section. Instantaneous point velocities u_z in the direction of the axis *Z* were measured just behind the end section (starting at 0.005 m from the end section). The average values of them representing the relevant components v_x and v_z of the (mean) point velocity was calculated; these components defined the (mean) point velocity *v* (see Figs 4 to 6).

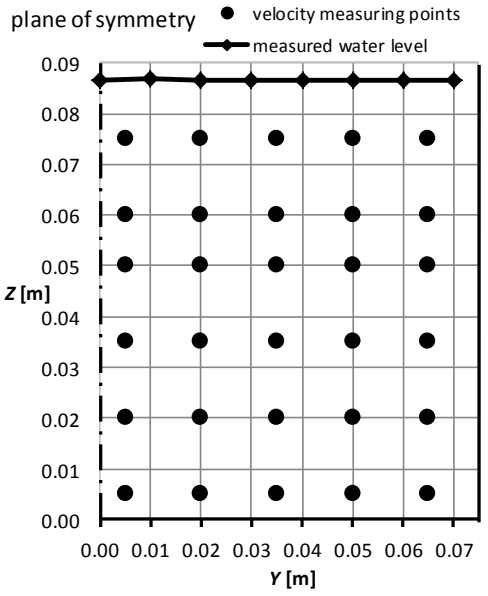

Fig. 4. Measured water surface level and the position of measurement of point velocities at the end section.

Measurement by a point contact gauge was made in three steps. The first step included the measurement of the position of the water surface level in a longitudinal plane of the channel from the end depth up to a distance of $X = -1.000$ m at 0.100 m intervals. These data were used to determine the position of the critical depth h_c, which was validated by us at a distance of $L_c = 3h_c$ (Fig. 1). The second step comprised the measurement of the water surface level at the end section. This measurement was made at 0.010 m intervals (Fig. 4). The level at the end section was detected as approximately horizontal. The shape of a half of the width of the free nappe was measured also (the symmetry about the plane *XZ* was assumed). Measurement was made in vertical sections spaced 0.010 m apart, up to a distance of $X = 0.300$ m and of the axis *Y* at 0.005 m intervals. At a distance greater than 0.300 m from the end section, the self-aeration of flow and the fluctuation of the water surface were so high. The shape of the nappe measured only by the upper and lower needle points is depicted in longitudinal planes *XZ* spaced 0.01 m apart (see Fig. 8).

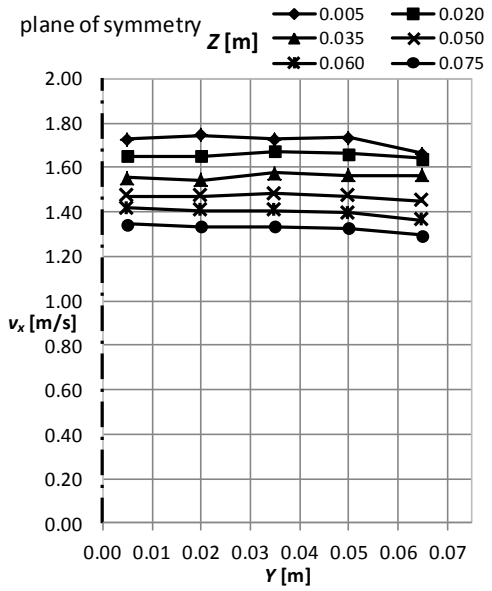

Fig. 5. *X* component of point velocity determined from measurement at the mid-profile of the end section.

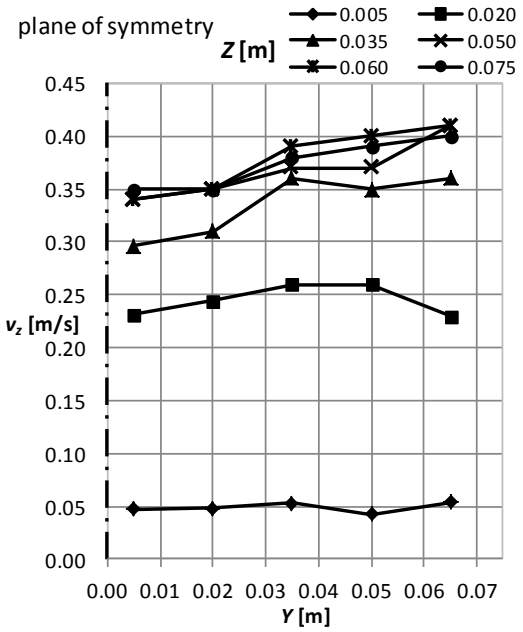

Fig. 6. *Z* component of point velocity determined from measurement at the mid-profile of the end section.

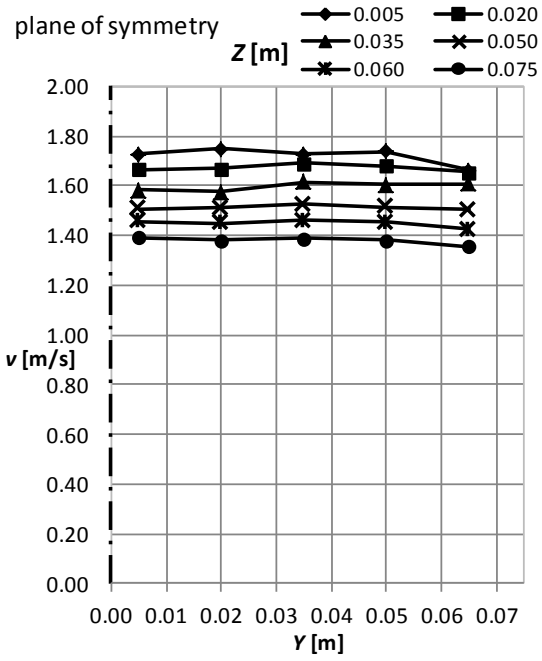

Fig. 7. Point velocity at the mid-profile of the end section.

The shape of the vertical cross section through the nappe gradually changes downstream along the centreline from an oblong shape up to the shape of a horseshoe (the shape of the nappe in the form of vertical sections at 0.05 m intervals is shown in Fig. 9). On a horizontal plan view, it widens along the axis *X* by about 8° and its thickness gradually reduces with the increasing mean flow velocity v_A. The upper surface of the nappe gradually all rounds; the lower surface of the nappe changes particularly in the places of its widening.

A surface characterizing the shape of a nappe was interpolated through the measured points. The shape of the nappe obtained in this way, with depicted vertical cross sections, is shown in dimensionless form in Fig. 10.

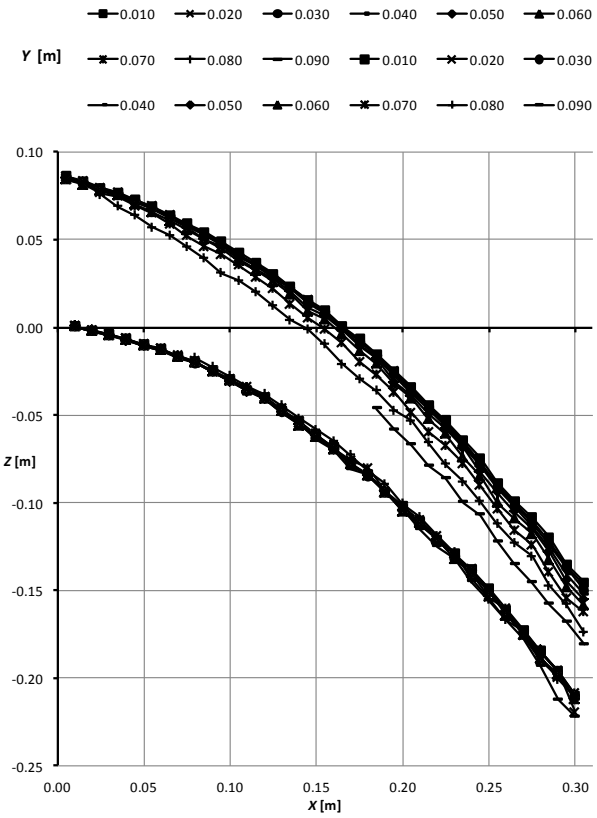

Fig. 8. Shape of a nappe measured by the upper and lower needle points, depicted in the longitudinal planes *XZ* with spacing of 0.01 m.

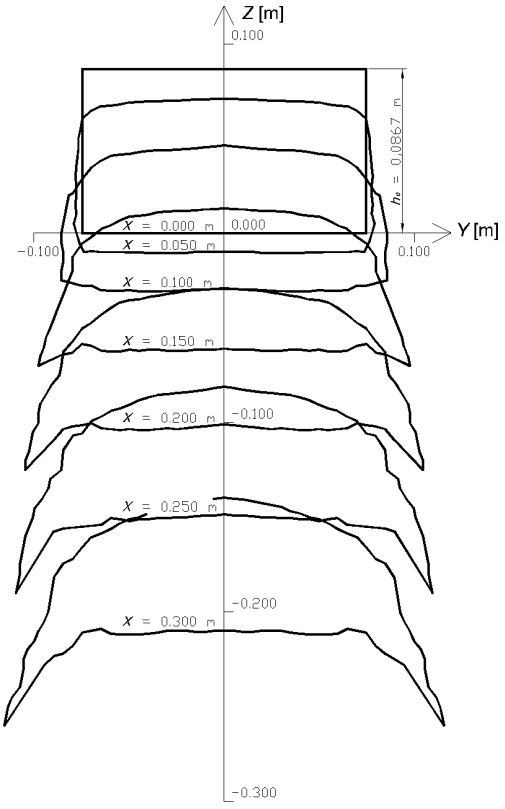

Fig. 9. Vertical cross sections through a nappe spaced 0.05 m apart in the direction of the axis *X*, evaluated from measurements.

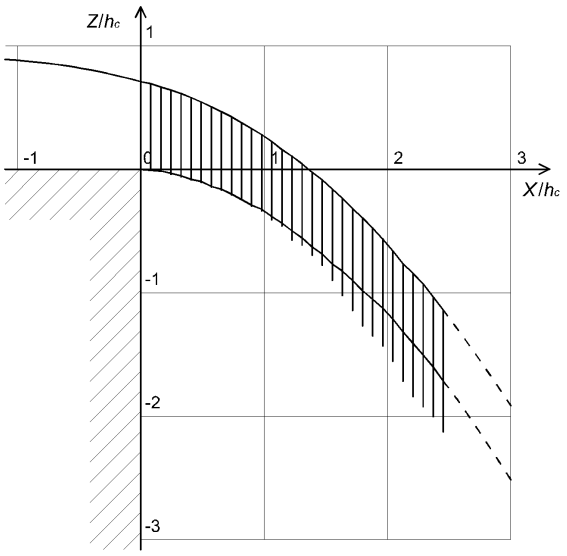

Fig. 10. Shape of a nappe evaluated from measurements – vertical cross sections and a longitudinal section through the plane *XZ*.

SHAPE DETERMINED BY CALCULATION

To determine the shape of a fully aerated and confined (Fig. 2) and an unconfined (Fig. 10) nappe by calculation, three approaches were used. The first approach was 1D (solving both a confined and an unconfined shape of a nappe) and was based on the characteristics of flow at the end section. The second approach was 2D in a vertical longitudinal plane (solving the confined shape of a nappe) and the third approach was 3D (solving the unconfined shape of a nappe).

1D calculation of the shape of a nappe on the basis of the characteristics of flow in the end section

This is a very simple method used to determine the shape of a nappe with a whole number of relatively significant simplified assumptions, but yielding relatively good results.
Assumptions for the calculation were as follows:

- The distribution of the point velocity v over the cross-sectional area A is constant. This simplification was used on the basis of the measurements of the velocity field made by us, which differed along the vertical within about 20% (compare Fig. 7). The centre of gravity of the velocity pattern is in the mid-depth h_e, being the origin of the centreline of the nappe.
- The pressure field does not affect flow in the nappe.
- The vector of the mean flow velocity v_A in the place of the centreline is in the mid-slope as is the slope of the water surface i_h at the same end section. This is based on the assumption of the linear distribution of velocity in the direction of the axis Z (the difference from the real pattern is shown in Fig. 8).
- The width b of the nappe fulfils one of the following conditions:
  - It is constant along its whole length (the nappe is confined); the space under the nappe is fully aerated; friction against the side walls is negligible; then the shape in a longitudinal section determined by calculation applies to the whole width of the nappe;
  - It is not constant along its whole length (the nappe is unconfined), but its relative width b/h is large and its inner part not affected by side widening (it is assumed that it does not widen: b = const.) has the same shape as a confined nappe, and hence the calculation applies only to this part;
  - It is not constant along its whole length (the nappe is unconfined), but its relative width b/h is small (the whole nappe is affected by widening), then it is assumed that the cross-sectional area through the nappe changes downstream from an oblong to a trapezium having the length of the upper edge unchanged and the length of the lower edge variable according to the widening of the nappe.
- The nappe is compact, does not break down and is not affected by friction against air or by surface tension.

The known variables are: the width b of the prismatic channel, the gravitational acceleration g, then either the end depth h_e or the critical depth h_c or the discharge Q, combined in the Eq. (1), the Eq. (2) and in the water level slope i_h at the end section (see certain methods in the chapter Free Overfall from a Channel or equations derived on the basis of experiments, e.g. in Davis et al., 1999, for broad-crested weirs Zachoval et al., 2012), or, for an unconfined nappe, the angle of its widening (if it is known for a particular case, e.g. in Emiroglu, 2010).

The procedure of the calculation consists of the determination of the mean flow velocity v_A at the end section with the width b of the cross-sectional area and the flow depth h_e

$$Q = v_A A_e = v_A b h_e . \tag{4}$$

The centreline slope i_s is determined from the water surface level slope i_h at the end section

$$i_s = 0.5 i_h . \tag{5}$$

Then, the velocity components are determined

$$i_s = \frac{v_{Az}}{v_{Ax}} , \tag{6}$$

$$v_A^2 = v_{Ax}^2 + v_{Az}^2 . \tag{7}$$

The pattern of the centreline of the nappe is solved in the time t. For the axis X it holds that

$$X = v_{Ax} t \tag{8}$$

and for the axis Z

$$Z = v_{Az} t + 0.5 \mathrm{g} t^2 . \tag{9}$$

The longitudinal shape of the nappe defined by the upper and lower surfaces is bound to its increasing mean flow velocity v_A of water due to the action of the gravitational acceleration g. Therefore, the thickness of the nappe along the length of its centreline is determined by using the Eq. of continuity (4) and the Eqs (7), (8) and (9) describing the trajectory of the centreline. The determination of the cross-sectional area A by applying the Eq. (4) along the length of the nappe depends on confinement of the nappe and its relative width b/h. In the case of a confined nappe, the width of an oblong cross section along the length of the centreline is the same, b = const. In the case of an unconfined and relatively wide nappe, the same is assumed for

the part unaffected by the side widening. In the case of an unconfined and relatively not so wide nappe, it is assumed that the cross section through the nappe changes downstream from an oblong to a trapezium that has its upper edge unchanging and the length of the lower edge variable according to the nappe widening (Emiroglu, 2010).

It is advantageous to create the shape of the nappe in a longitudinal plane of symmetry as an envelope of circles with their diameters equalling to the thickness of the nappe and with their centres on the centreline; the thickness of the nappe is constant over the cross section (Fig. 11).

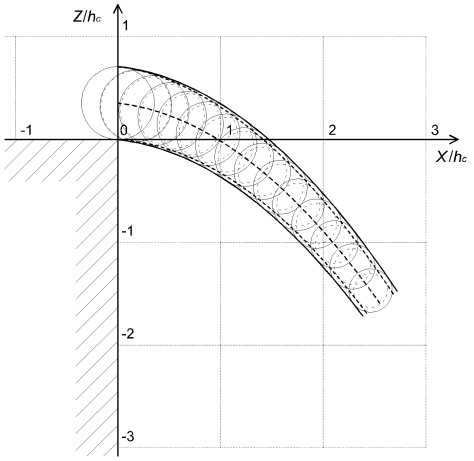

Fig. 11. Construction of the shape of a nappe, a 1D calculation, by a solid line – a confined nappe, or the part of an unconfined nappe unaffected by side widening, by a broken line – an unconfined nappe affected by side widening (input data from experiment).

2D calculation of the shape of a nappe

A 2D calculation of the shape of a nappe in a vertical plane assumes that the nappe is confined and the effect of the walls is negligible.

This calculation was made using the software ANSYS 12 – FLOTRAN (ANSYS, 2010) based on the finite element method. The Reynolds equations were solved using the Boussinesq approximation by introducing the turbulent viscosity ν_t that was determined by means of the standard k-ε model of turbulence. The water surface was calculated using the volume of fluid analysis. The mesh with quadrilateral elements was adjusted so that its use for water flow simulations could be maximized (Fig. 12 shows the boundaries of the mesh by a dashed line) and the gradients of variables could be well detected. The solution was time-dependent; it was necessary to adapt the length of the time step to the dimensions of the elements. The initial condition was the existence of water in all the elements. The boundary condition for the wall was the zero value of velocity; the condition of the external boundary was the zero reference pressure and the boundary condition on the inflow to the area was a predefined value of velocity. Because of the unicity of the setting and stability of the calculation, the last-mentioned boundary condition was solved as a pressure inflow with constant pressure and velocity over the cross section and with the upper level of the inflow by $0.1h$ lower than the assumed water surface level. The advantage of the setting was the constancy of the inflow velocity with the water surface level, and hence of its relation to pressure conditions as well. The condition of the possibility of the given setting was a sufficient length of the inlet part, in which stabilized flow conditions along the length developed. The length $50h_c$ was used. The solution is stable and converges relatively well. The extent of the mesh and the shape of the confined nappe determined by calculation are shown in dimensionless form in Fig. 12.

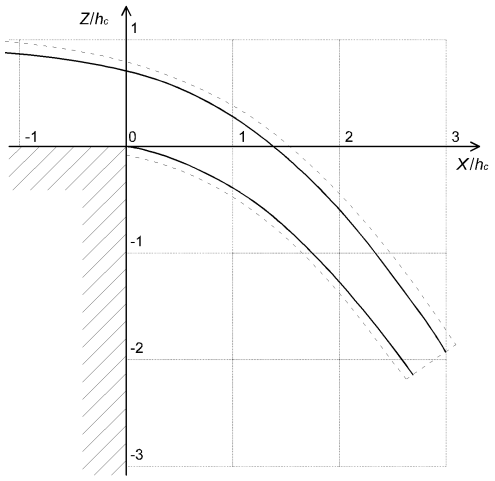

Fig. 12. 2D calculation of the shape of a nappe using the software ANSYS 12 – FLOTRAN, the shape of a nappe – by a solid line, the extent of the mesh – by a broken line.

3D calculation of the shape of a nappe

The calculation was made using the software ANSYS 12 – CFX (ANSYS, 2010) based on the finite volume method. The 3D calculation of the shape of a nappe uses a similar approach as in the case of the 2D calculation, but, in addition, solving the flow in the direction of the axis Y (hexahedral elements were used). A change, as compared with the above-given 2D approach, is the solution of the two-component water/air medium. The model of turbulence was identically used, as well as the setting of the boundary conditions except the expression of the effect of the wall in which the wall function was used, characterizing a hydraulically smooth wall. The position of the surface is determined by the ratio of water to air that equals to 0.5. The solution is stable. The shape of the unconfined nappe determined by calculation is shown in dimensionless form in Fig. 13.

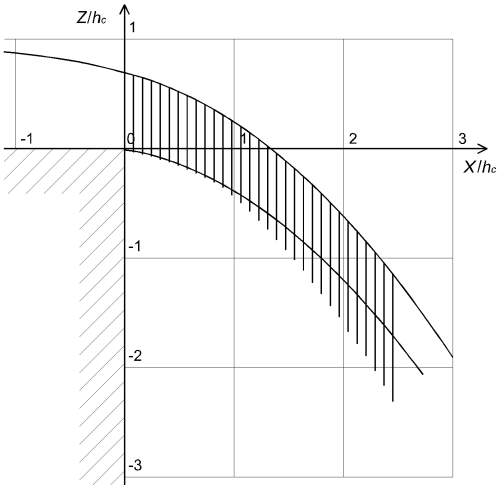

Fig. 13. 3D calculation of the shape of a nappe using the software ANSYS 12 – CFX, vertical cross sections through a nappe and a longitudinal section through the plane of symmetry XZ.

COMPARISON OF SHAPES

The shapes are compared for an unconfined as well as a confined fully aerated nappe.

The comparison of the shape of the confined fully aerated nappe determined by the 1D calculation and by the 2D calculation with the shape of the nappe determined by the Guidelines for Stabilising Waterways (Standing Committee on Rivers and Catchments, 1991) is shown in Fig. 14.

The comparison of the shape of the unconfined nappe determined by the 1D calculation and by 3D calculation with the shape of the nappe determined by measurement is shown in Fig. 16. To provide a better spatial picture of the shape of the nappe, a comparison is also made in the form of vertical sections spaced 0.05 m apart and of a longitudinal section through the plane of symmetry *XZ* in axonometric projection (Fig. 16).

The characteristics of the flow at the end section are fundamental for the subsequent determination of the shape of the nappe; therefore the distribution of the velocity field at the end section determined by the 2D calculation and by the 3D calculation is compared with the measured shape (Fig. 17). The picture shows certain dissimilarities in the shape of the velocity field determined by the 3D calculation in which the effect of friction against the side walls of the channel is significantly shown, which also explains the differences between the shape of the nappe determined by calculation and that determined by measurement (Fig. 16).

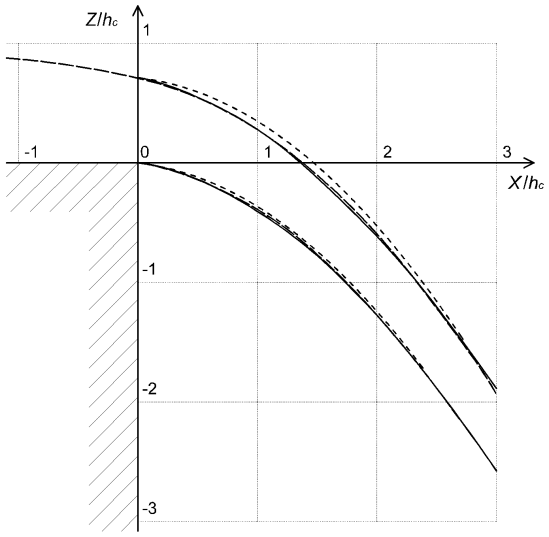

Fig. 14. Comparison of the shapes of a confined nappe determined by a 1D calculation – by a broken line, and by a 2D calculation – by a dashed line, with the shape determined by the Guidelines for Stabilising Waterways (Standing Committee on Rivers and Catchments, 1991) – by a solid line.

The discharges Q determined by different methods were also compared. The discharge $Q = 20.0$ l s^{-1} was calculated from the measurement of the determined point velocities v_i and their corresponding areas A_i at the end section according to the relation

$$Q = \sum_{i=1}^{n} \left(v_i \cdot A_i \right). \tag{10}$$

The discharge determined by the Thomson weir on the basis of the measurement of the overfall height was 20.1 l s^{-1}, and the discharge determined according to ISO 3847 on the basis of the measurement of the end depth h_e was 20.2 l s^{-1}. The discharge determined by the Thomson weir was always considered for all the numerical calculations.

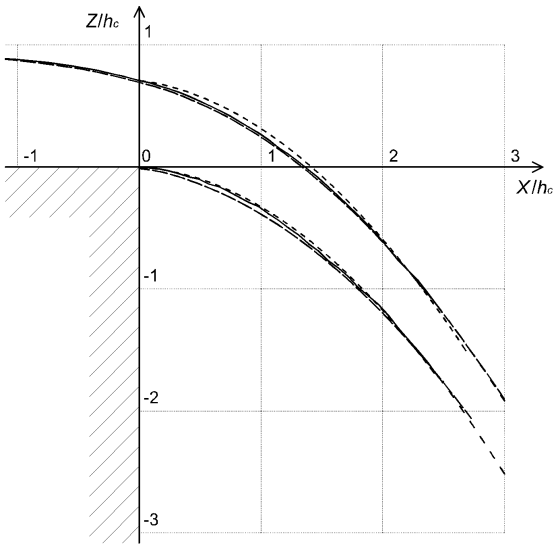

Fig. 15. Comparison of the shapes of an unconfined nappe determined by a 1D calculation – by a broken line, and by a 3D calculation – by a dashed line, with the shape determined by the measurement described in this paper – by a solid line, it applies for the plane of symmetry.

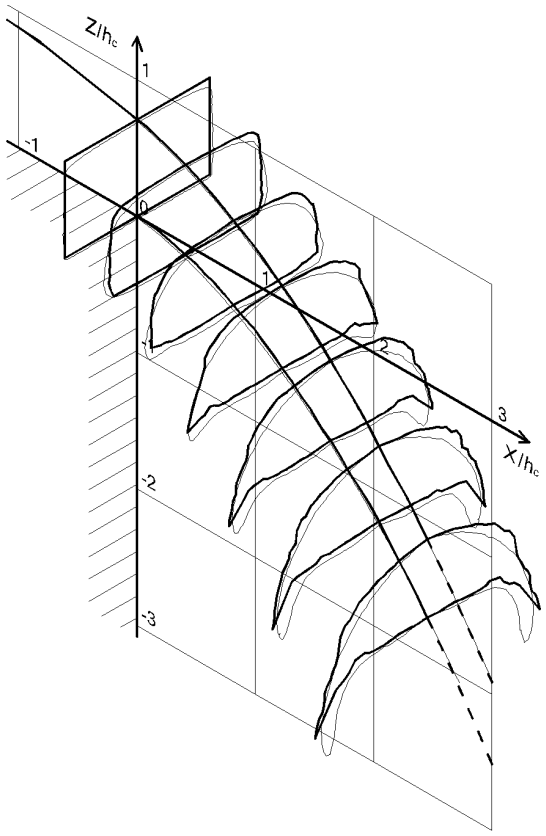

Fig. 16. Comparison of the shape of a nappe determined by measurement – by a thick line and by a 3D calculation – by a thin line in axonometric projection, vertical cross sections with horizontal spacing of 0.05 m and a vertical longitudinal section through the plane of symmetry.

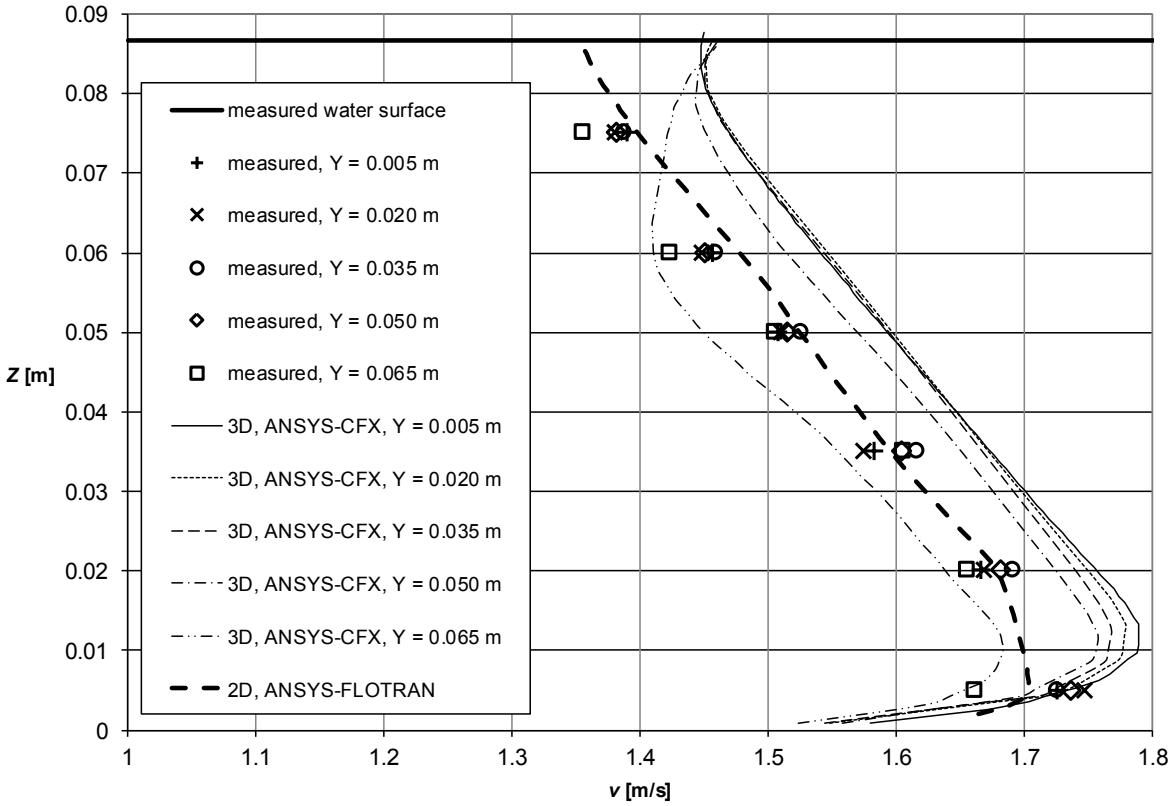

Fig. 17. Velocities in verticals at the end section.

CONCLUSIONS

The conclusions of the research can be summed up in the following points.

The shape of the confined and the unconfined overfall nappe unaffected by tailwater is markedly different in those cases in which the effect of confinement of the nappe by the sides is shown.

The 1D approach of the solution used, even despite its simplicity and considerable simplifications, yields relatively good results for the plane *XZ* in the cases of both the confined and the unconfined nappe and can be used, e.g., for the primary design of an object or its part. Because of the 1D approach, however, it does not provide a spatial view of the shape of a nappe, which is an essential restriction particularly in the case of an unconfined nappe. It is possible to use it for the preliminary design of structures with a confined, fully aerated and compact nappe and with smooth guiding side walls where the effect of the curvature of the nappe in the cross section can be neglected. In comparison with 1D more sophisticated methods for confined nappe this very simple method gives approximately similar accurate results.

The 2D approach describes the shape of a confined nappe better than the 1D approach, provides complete information about the distribution of pressure and velocity in the longitudinal plane through the nappe, but does not yield a view of the cross shape of the nappe either. It can be recommended for use in designing objects with smooth side walls bounding a compact nappe where the curvature of the nappe in the cross section can be neglected.

The 3D approach yields the most accurate results with a complete description of velocities and pressures in a nappe. It is possible to recommend it for the design of objects with a confined as well as unconfined and compact nappe.

It is necessary to emphasize that in general cases surface tension, the aeration of the flow and the roughness of the walls of a channel have significant effects on the shape of an overfall nappe. These effects were neglected within the numerical solution in the tested cases.

The velocity field at the end section is practically identically described using numerical models; in the 3D calculation, the effect of the side walls of a channel appears to be greater (the near-wall area is thicker).

Acknowledgements. Thanks are due to Project GA103/09/0977 – Experimental and Numerical Modelling of Turbulent Flow with Massive Separation (2009–2012).

REFERENCES

Ali, K.H.M., Sykes, A., 1972. Free-vortex theory applied to free overfall. Journal of Hydraulics Division, ASCE, 98(5), 973–979.

Anderson, M.V., 1967. Non-uniform flow in front of a free overfall. Acta Polytechnica Scandinavica, 42, 1–24.

ANSYS 12, 2010. www.ansys.com.

Beirami, M.K., Nabavi, S.V., Chamani, M.R., 2006. Free overfall in channels with different cross sections and sub-critical flow. Iranian Journal of Science & Technology, Transaction B, Engineering, 30, B1.

Bos, M.G., 1989. Discharge Measurement Structures. Third revised edition. Publication 20. ILRI. ISBN 90 70754 15 0.

Böhm, P., 2010. Shape of a Free Water Jet Overflowing from a Rectangular Channel. Brno, pp. 61, Brno University of Technology. Faculty of Civil Engineering. Institute of Water Structures.

Castro-Orgaz, O., Hager, W.H., 2010. Moment of momentum equation for curvilinear freesurface flow. Journal of Hydraulic Research, 48, 5, 620–631.

Castro-Orgaz, O., Hager, W.H., 2011. Vorticity equation for the streamline and the velocity profile. Journal of Hydraulic Research, 49, 6, 775–783.

Chow, V.T., 1959. Open-Channel Hydraulics. McGraw-Hill, New York.

Davis, A.C., Ellet, B.G.S., Jacob, R.P., 1998. Flow measurement in sloping channels with rectangular free overfall. Journal of Hydraulic Engineering, ASCE, 124(7), 760–763.

Davis, A.C., Jacob, R.P., Ellett, G.S., 1999. Estimating trajectory of free overfall nappe. Journal of Hydraulic Engineering, 125, 79–82.

Dey, S., 2000. End depth in steeply sloping rough rectangular channels. Sadhana, 25, Part 1, 1–10.

Dey, S., 2001. Flow measurement by the end-depth method in inverted semicircular channels. Flow Measurement and Instrumentation, 12, 253–258.

Dey, S., 2002. Free overall in open channels: state-of-the-art review. Flow Measurement and Instrumentation, 13, 247––264.

Dey, S., 2002a. Free overall in circular channels with flat base: a method of open channel flow measurement. Flow Measurement and Instrumentation, 13, 209–221.

Dey, S., Kumar, B., 2002. Hydraulics of free overfall in 1-shaped channels. Sadhana, 27, Part 3, 353–363.

Dey, S., Lambert, M.F., 2006. Discharge prediction in compound channels by end depth method. Journal of Hydraulic Research, 44, 6, 767–776.

Emiroglu, M.E., 2010. Estimating flow characteristics of different weir types and optimum dimensions of downstream receiving pool. Journal of Hydrology and Hydromechanics, 58, 4, 245–260.

Falvey, H.T., 1980. Air-Water Flow in Hydraulic Structures. United states Department of the Interior, Water and Power Resources Service. Engineering Monograph, 41.

Ferro, V., 1999. Theoretical end-depth-discharge relationship for free overfall. Journal of Irrigation and Drainage Engineering, Vol. 44, 40–44.

Firat, C.E., 2004. Effect of Roughness on Flow Measurements in Sloping Rectangular Channels with Free Overfall. Thesis. THE Middle East Technical University.

Hager, W.H., 1983. Hydraulics of the plane overfall. Journal of Hydraulic Engineering, ASCE, 109(12), 1683–1697.

Hong, Y., Huang, H., Wan, S., 2010. Drop characteristics of free-falling nappe for aerated straight-drop spillway. Journal of Hydraulic Research, 48, 1, 125–129.

ISO 3847, 1977. Measurement of liquid flow in open channels by weirs and flumes – End-depth method for estimation of flow in rectangular channels with a free overfall.

ISO 4371, 1984. Measurement of liquid flow in open channels by weirs and flumes – End-depth method for estimation of flow in non-rectangular channels with a free overfall (approximate method).

Jia, Y., Wang, S.Y., 2005. Numerical model validation using physical model data. US-CHINA Workshop on Advanced Computational Modelling in Hydroscience & Engineering, Oxford, Mississippi, USA. 1–10.

Kolář, V., Patočka, C., Bém, J., 1983. Hydraulics. SNTL, Praha. (In Czech.)

Marchi, E., 1993. On the free overfall. Journal of Hydraulic Research, 31, 6, 777–790.

Markland, E., 1965. Calculation of flow at a free overfall by relaxation method. ICE Proceedings, 31, 71–78.

Murty Bhallamudi, S., 1994. End depth in trapezoidal and exponential channels. Journal of Hydraulic Research, 32(2), 219–232.

Pařílková, J., Říha, J., Zachoval, Z., 2012. The influence of roughness on the discharge coefficient of a broad-crested weir. Journal of Hydrology and Hydromechanics, 60(2), 101–114.

Raikar, R.V., Kumar, D.N., Dey, S., 2004. End depth computation in inverted semicircular channels using ANNs. Flow Measurement and Instrumentation, 15, 285–293.

Ramamurthy, A.S., Qu, J., Vo, D., 2006. VOF model simulation of a free overfall in trapezoidal channels. Journal of Irrigation and Drainage, 132, 4, 425–428.

Rouse, H., 1936. Discharge characteristics of the free overfall. Civil Engineering, ASCE, 6(4), 257–260.

Sharifi, S., Sterling, M., Knight, D.W., 2010. Prediction of end-depth ratio in open channels using genetic programming. Journal of Hydroinformatics, 13, 1, 36–48.

Southwell, R.V., Vaisey, G., 1946. Relaxation methods applied to engineering problems: XII, Fluid motions characterized by free stream-lines. Philosophical Transactions of the Royal Society, 240, 815, 117–161.

Standing Committee on Rivers and Catchments, 1991. Guidelines for Stabilising Waterways. Straight drop structure. Design Guidelines. Australia, Victoria.

Wahl, T.L., Frizell, K.H., Cohen, E.A., 2008. Computing the trajectory of free jets. Journal of Hydraulic Engineering, 134, 2, 256–260.

Wang, S.S.Y., Roche, P.J., Schmalz, R.A., Jia, Y., Smith, P.E., 2009. Verification and Validation of 3D Free-Surface Flow Models. ASCE, 2009. ISBN 978-0-7844-0957-2.

White, P., Bakhmeteff, B.A., Feodoroff, N.V., Kindsvater, C.E., Christiansen, J.E., Hall, L.S., Rouse, H., 1943. Discussion of energy loss at the base of a free overfall. Transactions of the American Society of Civil Engineers, 108, 1, 1383–1387.

Zachoval, Z., Mistrová, I., Roušar, L., Šulc, J., Zubík P., 2012. Zone of flow separation at the upstream edge of a rectangular broad-crested weir. Journal of Hydrology and Hydromechanics, 60, 4, 288–298.

Zerihun, Y.T., Fenton, J.D., 2004. Boussinesq-type momentum equations solutions for steady rapidly varied flows. Advances in Hydro-Science and -Engineering, 6, 1–10.

Received 8 June 2011
Accepted 6 December 2012